Strong-field terahertz optical mixing in excitons

M. Y. Su,* S. G. Carter, and M. S. Sherwin
Physics Department and Center for Terahertz Science and Technology, University of California, Santa Barbara, California 93106

A. Huntington and L. A. Coldren
Materials Department, University of California, Santa Barbara, California 93106

(Received 8 January 2003; published 17 March 2003)

Driving a double-quantum-well excitonic intersubband resonance with a terahertz (THz) electric field of frequency ω_{THz} generated terahertz optical sidebands $\omega=\omega_{THz}+\omega_{NIR}$ on a weak near-infrared probe. At high THz intensities, the intersubband dipole energy which coupled two excitons was comparable to the THz photon energy. In this strong-field regime, the sideband intensity displayed a nonmonotonic dependence on the THz field strength. The oscillating refractive index which gives rise to the sidebands may be understood by the formation of dressed states that oscillate with the same periodicity as the driving THz field.

DOI: 10.1103/PhysRevB.67.125307 PACS number(s): 78.70.−g, 42.65.−k, 73.21.Fg

I. INTRODUCTION

Intense light fields can mix with quantum states of matter to form dressed states. Observed manifestations of dressed states in semiconductors include Rabi oscillations[1,2] and electromagnetically induced transparency.[3,4] In these effects, a resonant optical field is strong enough to overcome processes which dephase the coherent coupling of two semiconductor states by the field. More precisely, the Rabi frequency $\mu E/\hbar$ is greater than the dephasing rate γ: $\mu E>\hbar\gamma$, where μ is the dipole moment and E is the electric field strength. However, at optical frequencies the Rabi energy is typically much smaller than the resonant photon energy: $\mu E\ll\hbar\omega$. If the field strength is increased further, a *strong-field* regime is encountered as the Rabi energy becomes comparable to the photon energy,

$$\mu E\geqslant\hbar\omega. \tag{1}$$

There are many theoretical studies[5–8] of bound electronic states of semiconductors subject to laser fields in the limit of Eq. (1). These studies predict shifts and splittings in absorption lines as well as nonmonotonic power dependences of nonlinear mixing. However, we are aware of no experimental work in this regime.

We performed strong-field experiments in which a weak near-infrared (NIR) probe-laser beam was mixed with a strong terahertz (THz) pump beam in a gated, asymmetric double quantum well (DQW). The THz field coupled to an excitonic intersubband excitation while the NIR field coupled to an excitonic interband excitation. Applying a dc voltage to the gates brought the intersubband transition into resonance with the THz field, and the interband transition into resonance with the NIR field. When these resonance conditions were met, the NIR probe was modulated resulting in the emission of optical sidebands which appeared at frequencies $\omega_{sideband}=\omega_{NIR}+n\omega_{THz}$ where ω_{NIR} (ω_{THz}) is the frequency of the NIR (THz) beam and $n=\pm1,2,\ldots$.

The $n=1$ sideband is a more sensitive probe for strong-field effects than shifts in excitonic absorption lines, as it is a zero-background measurement in two respects. First, there is no sideband when the THz pulse is not present. Second, there is no contribution to the sideband from any THz polarization component which is not in the growth direction, where the asymmetry of the DQW relaxes the usual selection rule for odd sidebands. This paper describes a strong-field THz interaction between confined exciton states, which manifested itself as a nonmonotonic dependence of the $n=1$ sideband intensity on THz field strength.

II. EXPERIMENT AND RESULTS

The sample consisted of an active region, gates, and a distributed Bragg reflector (DBR). The active region consisted of 5 periods of DQW, each consisting of a 120-Å GaAs QW and a 100-Å GaAs QW separated by a 25-Å $Al_{0.2}Ga_{0.8}As$ tunnel barrier. Each period was separated by a 300-Å $Al_{0.3}Ga_{0.7}As$ barrier. The dimensions of the DQW were designed so that the two lowest-lying electron subbands were separated by ≈10 meV (≈2.4 THz) at flat band. Around this frequency, (1) can be satisfied using our THz source, the Free Electron Laser (FEL) at the University of California, Santa Barbara. Within the 10 meV energy splitting constraint, the degree of inversion-asymmetry was designed to maximize the second-order nonlinear susceptibility ($\chi^{(2)}$) near flat band conditions.

The active region was sandwiched between two gates, each consisting of a Si δ doped 70-Å QW with carrier density $\approx1\times10^{12}$ cm^{-2}. The gates were separated from the active region by 3000-Å $Al_{0.3}Ga_{0.7}As$ barriers. Since the gate QW's were much narrower than the active DQW's, the gate QW's were transparent to both the THz and NIR beams.

The gated DQW's were grown on top of a DBR that consisted of 15 periods of 689-Å AlAs and 606-Å $Al_{0.3}Ga_{0.7}As$. It had a low-temperature passband nearly centered on the low-temperature band gap of the DQW, making it about 95% reflective for the NIR probe beam and sidebands.

We etched a mesa and annealed NiGeAu ohmic contacts to the gate QW's. The sample was then cleaved into a ($0.5\times1\times8$)-mm chip. A ($0.5\times1\times5$)-mm strip of crystal sapphire, with the optically slow axis along the long dimension, was mechanically pressed against the surface of the sample

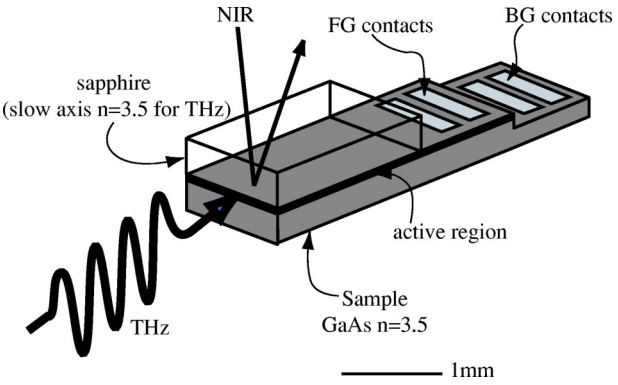

FIG. 1. Processed waveguide device and optical coupling scheme.

with a beryllium copper clip as shown in Fig. 1. The sample was cooled to 21 K in a closed-cycle He cryostat. At cryogenic temperatures, sapphire was index matched to GaAs and transparent at THz and NIR wavelengths, thus forming a heavily overmoded waveguide with the epilayer in the middle. This resulted in higher fields at the active region than was possible without the sapphire, where the active region would be at the edge of a dielectric waveguide.

The full power of THz beam was 1 kW at 2.5 THz, as measured by a calibrated pyroelectric detector. The beam was polarized in the growth direction, propagated in the QW plane and focused by a 90° off-axis parabolic mirror (F/1) into the edge of the waveguide. The THz power incident on the sample could be continuously varied by a pair of wire-grid polarizers. The power was monitored by a pyroelectric detector which enabled an accurate measurement of relative THz field strengths. However, since the exact size of the THz mode in the waveguide was difficult to measure, the absolute THz electric field scale at full power must be estimated. An extreme lower bound of 4 kV/cm assumes a mode that fills the 1-mm square cross section of the waveguide. This condition exists if the sideband generation does not depend on the position of the NIR probe along the length of the waveguide. An extreme upper bound of 28 kV/cm assumes a diffraction-limited spot size at 2.5 THz. In this case, the device is not acting as a waveguide, so the sideband should decay when the NIR probe is moved by the length of a THz beam waist. Since the actual experimental conditions were well within the two extremes, we estimated the maximum THz electric-field strength to be between 5 and 20 kV/cm.

NIR light from a continuous-wave Ti:Sapphire laser was chopped by an acousto-optic modulator into 25-μs pulses which overlapped the 5-μs FEL pulses at maximum repetition rate of 1.5 Hz. The vertically polarized NIR beam propagated normal to the THz beam, and was focused (F/10) at a power density of ≈ 5 W/cm^2. Absorption measurements indicated that the maximum photo excited carrier density was less than 1×10^9 cm^{-2} per quantum well. The reflected beam, sidebands, and photoluminescence (PL) were analyzed by a second polarizer, dispersed by a 0.85-m double monochromator, and detected by a photomultiplier tube.

The emitted sideband always had the same polarization state as the incident NIR beam. There were no detectable

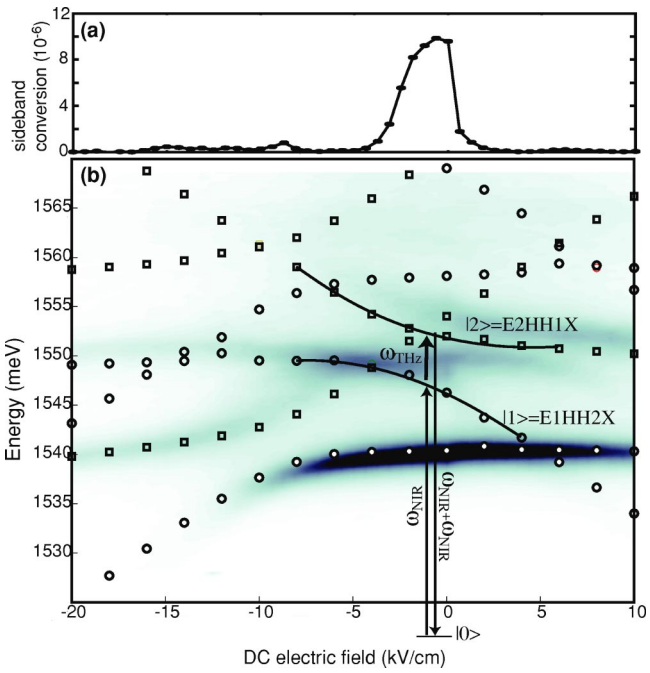

FIG. 2. (a) dc electric-field dependence of the sideband intensity at $\hbar\omega_{NIR}=1547$ meV and $\omega_{THz}=1.5$ THz (6.2 meV). (b) Experimental PL spectra as a function of dc electric field. Theoretical E1HH$_\nu$X and E2HH$_\nu$X energies are indicated by circles and squares, respectively. The overlaid diagram illustrates the resonance measured in (a) where the NIR field is resonant with the E1HH2X exciton and the THz field resonantly couples the E1HH2X and E2HH1X excitons.

sidebands when the THz polarization was rotated parallel to the plane of the DQW.

The sideband generation process displayed a pronounced resonance as a function of dc electric field [Fig. 2(b)]. The enhancement occured when the NIR field resonantly coupled the vacuum state $|0\rangle$ with an exciton $|1\rangle$, and the THz field resonantly coupled a transition between excitons $|1\rangle$ and $|2\rangle$.

The exciton states of DQW's in a dc electric field are well understood.[9–12] They can be labeled as E$_\mu$HH$_\nu$X, indicating an exciton consisting of an electron in conduction subband μ and a heavy hole in valence subband ν. The PL spectra as a function of applied dc electric field are shown in Fig. 2(b). The E$_\mu$HH$_\nu$X exciton energies were calculated variationally in the effective mass approximation and are overlaid on the PL. Changing the dc electric field tuned the excitonic intersubband transition into resonance with the THz field, as shown in the overlaid resonance diagram in Fig. 2(b). Detailed spectroscopy of the excitonic intersubband resonance was performed by studying the sideband generation as a function of THz frequency, NIR frequency, and dc electric field. The spectroscopic results are presented elsewhere.[13,14] The sideband resonance targeted for strong-field studies in this paper was E1HH2X-E2HH1X, a peak assignment made by comparing low-field sideband spectroscopy with a nonlinear susceptibility calculation for excitons.

The dependence on THz field strength of sideband generation at various THz frequencies is shown in Fig. 3. Each curve was taken at a gate bias near the E1HH2X-E2HH1X

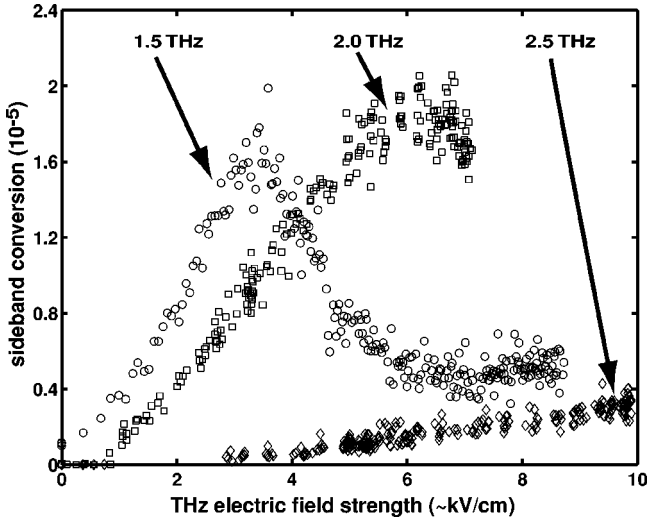

FIG. 3. Resonant THz field strength dependence of sideband generation at 1.5 THz, 2.0 THz, and 2.5 THz (6.2 meV, 8.2 meV, 10.4 meV). The absolute THz electric-field scale is accurate only to within a factor of 2.

resonance.[13] The most striking feature was the nonmonotonic behavior in the strong-field regime when the Rabi energy was comparable to the photon energy. Clearly at lower frequencies, the power dependence rolled over at a lower-field strength, as would be expected from the relationship (1).

By sitting at the peak NIR frequency for E1HH2X-E2HH1X and varying the dc gate voltage, we took THz power-dependence scans at various THz detunings $E_2-E_1-\hbar\omega_{THz}$ where E_2 (E_1) is the energy of the upper (lower) exciton state. The shape of the THz field dependence varied strongly with the detuning (Fig. 4).

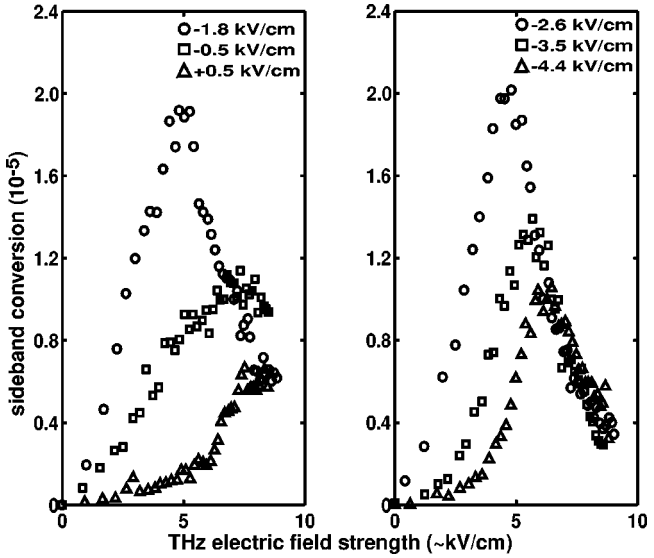

FIG. 4. THz field strength dependence of $n=1$ sideband for $\omega_{NIR}=1548$ meV, $\omega_{THz}=1.5$ THz (6.2 meV) at various dc electric-field detunings from the resonance condition illustrated in Fig. 2. The absolute THz electric-field scale is accurate only to within a factor of 2.

III. THEORY

In a typical optical mixing experiment the laser fields are a small perturbation on the nonlinear medium, and are thus modeled using a nonlinear susceptibility, $\chi^{(2)}$. The power dependence in Figs. 3 and 4 cannot be explained with a $\chi^{(2)}$. Saturation effects from a nonlinear susceptibility[15] can only come about when contributions from virtual transitions initiated from excitons $E_\mu HH_\nu X$ are comparable to those initiated from the vacuum $|0\rangle$. However, with our undoped sample and weak NIR beam, the population of excitons ($<10^9$ cm^{-2}) was several of orders magnitude smaller than the density of carriers in the valence band. Therefore, a nonlinear susceptibility can only predict a linear dependence of sideband intensity on THz power (i.e., a quadratic dependence on field strength). In addition, Coulomb screening and Pauli exclusion effects are not issues, since quantum well excitons are noninteracting at densities below 10^{11} cm^{-2}.[16,17]

The physical cause of the roll over in power dependence can be understood from the point of view of frequency modulation of the NIR probe as it passes through an oscillating index of refraction. In the case of a purely sinusoidal frequency modulation, the amplitude of the $n=1$ sideband rolls over when the modulation depth $\Delta\omega$ is twice the modulation frequency ω_{THz}. The actual functional form of the power dependence is far more complicated than a simple Bessel function, since many harmonics of the THz field exist, and the relationship between Rabi energy and modulation depth is nontrivial.

The following model captures qualitative features of the dependence of sidebands on THz power by treating the interaction of the THz field with exciton states in a nonperturbative manner. The Hamiltonian is

$$H=H_0+zE_\omega\cos\omega t+x\lambda E_\Omega\cos\Omega t \tag{2}$$

where H_0 is the exciton Hamiltonian, E_ω is the strong THz electric field, E_Ω is the weak NIR electric field, and z and x are dipole operators.

The exciton Hamiltonian H_0 and the dipole operators are treated phenomenologically. H_0 has eigenstates $\phi_0(x,z)$, $\phi_1(x,z)$, and $\phi_2(x,z)$ with eigenenergies $E_0=0$, E_1, and E_2, respectively. The polarization selection rules for creating and coupling excitons lead to the dipole matrices

$$z=\begin{pmatrix}0&0&0\\0&0&z_{12}\\0&z_{21}&z_{22}\end{pmatrix},\quad x=\begin{pmatrix}0&x_{01}&x_{02}\\x_{10}&0&0\\x_{20}&0&0\end{pmatrix}.$$

The nonzero terms $x_{\alpha\beta}=\langle\phi_\alpha|x|\phi_\beta\rangle$ and $z_{\alpha\beta}=\langle\phi_\alpha|z|\phi_\beta\rangle$ are set equal to unity.

For $\lambda=0$, the solutions $\varphi_i(z,t)$ of the Schrodinger equation with the Hamiltonian (2) oscillate with frequency components at harmonics of ω.[18] The oscillation of the wave function leads directly to an oscillating refractive index which modulates the weak NIR probe.

Expanding the spatial dependence of $\varphi_i(z,t)$ in terms of the original exciton eigenstates $\phi_\alpha(z)$, yields

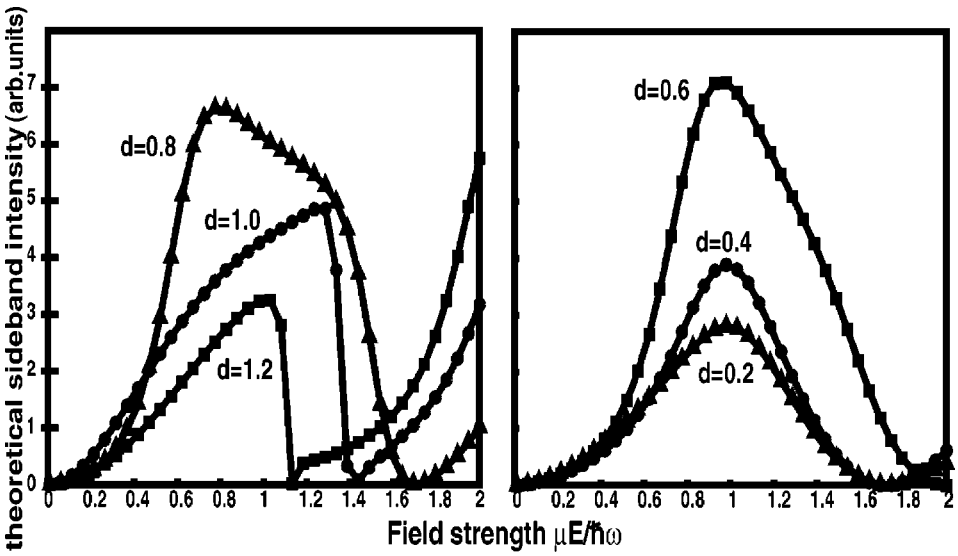

FIG. 5. Sidebands calculated by evaluating the square of Eq. (7) at various detuning parameters. Left, $d=(E2-E1)/\hbar\omega=0.8,1.0,1.2$; Right, $d=(E2-E1)/\hbar\omega=0.2,0.4,0.6$.

$$\varphi_i(z,t)=e^{-i\epsilon_i t/\hbar}\sum_{\alpha,n} c^i_{\alpha,n}e^{-in\omega t}\phi_\alpha(z). \tag{3}$$

The coefficients $c^i_{\alpha,n}$ determine the parts of the index of refraction which oscillate at particular multiples of ω. These Floquet coefficients are closely related to the photon-assisted tunneling sidebands, which appear in the irradiated current-voltage curves in superconducting weak-link junctions[19] and coupled quantum wells.[20]

The states $\varphi_i(z,t)$ (3) are solved nonperturbatively by diagonalizing the Floquet matrix F associated with the Hamiltonian[6,7] (2) for $\lambda=0$. The Floquet matrix is given by

$$F=\begin{pmatrix} \ddots & [z] & 0 & 0 & 0 \\ [z] & [H_0]-\hbar\omega & [z] & 0 & 0 \\ 0 & [z] & [H_0] & [z] & 0 \\ 0 & 0 & [z] & [H_0]+\hbar\omega & [z] \\ 0 & 0 & 0 & [z] & \ddots \end{pmatrix}, \tag{4}$$

where $[H_0]$ and $[z]$ are matrix representations of the operators H_0 and z in the $|\phi_\alpha\rangle$ basis. In practice, the Floquet matrix (4) must be truncated up to $\pm N$ photons, where N can be made arbitrarily large for an arbitrarily precise result at high-field strengths. Here we use $N=16$ photons.

The dipole response of $\varphi_i(z,t)$ to the weak NIR probe is determined by calculating the expectation value of $x(t)$ using standard first-order time-dependent perturbation theory. The $+1\omega$ sideband is given by the Fourier component of $x(t)$ oscillating at the frequency $\Omega+1\omega$.

Discarding second-order terms and antiresonant contributions, the dipole expectation is given by

$$\langle\psi|x|\psi\rangle=E_\Omega e^{-i\Omega t}\sum_{i=1}^{2}\frac{\langle\varphi_0|x|\varphi_i\rangle\langle\varphi_i|x|\varphi_0\rangle}{\epsilon_i-\hbar\Omega}. \tag{5}$$

The form of Eq. (5) is the same as the linear susceptibility of an undriven system, except the states φ_i are oscillating Floquet states instead of stationary states. Explicitly expanding the Floquet states in the numerator gives us an expression for the polarization

$$\langle x(t)\rangle=E_\Omega e^{-i\Omega t}\sum_{i=1}^{2}\sum_{\substack{n,\alpha\\ m,\beta}}\frac{c^i_{n,\alpha}c^i_{m,\beta}e^{-i(n-m)\omega t}x_{0\beta}x_{\alpha 0}}{\epsilon_i-\hbar\Omega}. \tag{6}$$

The $+1\omega$ sideband is given by the Fourier component of $x(t)$ oscillating at the frequency $\Omega+1\omega$. Also, for the resonant condition illustrated in Fig. 2, $\hbar\omega\approx\epsilon_1$, so we keep only the $i=1$ term in the sum (6). This condition is satisfied when $n-m=1$. The resulting expression for the sideband polarization is thus proportional to the products of neighboring Fourier components:

$$x_{sideb\ \text{and}}(t)=\frac{E_\Omega e^{-i(\Omega+\omega)t}}{\epsilon_1-\hbar\Omega}\sum_{n,\alpha,\beta}c^1_{n+1,\alpha}c^1_{n,\beta}x_{0\beta}x_{\alpha 0}. \tag{7}$$

The intensity of the sideband is proportional to $x^2_{sideband}$, which is plotted versus field strength for various detunings in Fig. 5. The detuning parameter d is the level spacing normalized by the photon energy of the strong field, $d=(E2-E1)/\hbar\omega$.

Our model captures the rollover of the resonant power dependence up to field strengths of around $\mu E/\hbar\omega\approx 1.5$. Given a calculated excitonic intersubband dipole of $\mu/e=12$ nm,[14] the strong-field condition is met at a THz field of 5 kV/cm. Experimentally the sideband never completely disappeared, a striking prediction of the theory. It is unlikely that a three-state simplification is entirely valid because there is a spectrum of other exciton states as well as an electron-hole continuum that may provide significant off-resonant contributions.

IV. CONCLUSION

We drove a quantum-well excitonic intersubband transition with an intense THz laser field and monitored an optical

sideband generated by the nonlinear mixing between the THz field and a weak NIR probe. When the THz power was increased to a regime where the Rabi energy was comparable to the photon energy, the sidebands displayed a nonmonotonic dependence on THz power. The THz power at which the sideband intensity rolled over increased with THz frequency, and the specific shape of the power dependence could be varied by detuning the excitonic intersubband transition with an applied dc electric field. The unusual power dependence indicated that the exciton states were strongly dressed and oscillated at multiple harmonics of the driving THz field. The strength of the sideband was determined by the amplitudes of neighboring harmonics, which we calculated nonperturbatively within the Floquet formalism.

ACKNOWLEDGMENTS

This research was funded by Grant No. NSF-DMR 0070083.

*Present address: National Institute of Standards and Technology, 325 Broadway, Boulder, CO 80305.

[1] B.E. Cole, J.B. Williams, B.T. King, M.S. Sherwin, Nature (London) **410**, 60 (2001).
[2] T.H. Stievater, X. Li, D.G. Steel, D. Gammon, D.S. Katzer, D. Park, C. Piermarocchi, L.J. Sham, Phys. Rev. Lett. **87**, 133603 (2001).
[3] S.E. Harris, J.E. Field, and A. Imamoglu, Phys. Rev. Lett. **64**, 1107 (1990).
[4] G.B. Serapiglia, E. Paspalakis, C. Sirtori, K.L. Vodopyanov, and C.C. Phillips, Phys. Rev. Lett. **84**, 1019 (2000).
[5] B. Birnir, B. Galdrikian, R. Grauer, and M.S. Sherwin, Phys. Rev. B **47**, 6795 (1993).
[6] K. Johnsen and A.-P. Jauho, Phys. Rev. Lett. **83**, 1207 (1999).
[7] T. Fromherz, Phys. Rev. B **56**, 4772 (1997).
[8] A.V. Maslov and D.S. Citrin, Phys. Rev. B **62**, 16 686 (2000).
[9] J. Soubusta, R. Grill, P. Hlidek, M. Zvara, L. Smrcka, S. Malzer, W. Geselbrecht, and G.H. Dohler, Phys. Rev. B **60**, 7740 (1999).
[10] V.V. Krivolapchuk, E.S. Moskalenko, A.L. Zhmodikov, T.S. Cheng, and C.T. Foxon, Fiz. Tverd. Tela (Leningrad) **41**, 291 (1999).
[11] T. Kamizato and M. Matsuura, Phys. Rev. B **40**, 8378 (1989).
[12] T. Westgaard, Q.X. Zhao, B.O. Fimland, K. Johannessen, and L. Johnsen, Phys. Rev. B **45**, 1784 (1992).
[13] M.Y. Su, S. Carter, M.S. Sherwin, A. Huntington, and L.A. Coldren, Appl. Phys. Lett. **81**, 1564 (2002).
[14] M. Y. Su, Ph.D. thesis, University of California, Santa Barbara, 2002.
[15] R. Boyd, *Nonlinear Optics* (Academic, San Diego, 1992).
[16] S. Schmitt-Rink, D.S. Chemla, and D.A.B. Miller, Phys. Rev. B **32**, 6601 (1985).
[17] K.-H. Schlaad, Ch. Wever, J. Cunningham, C.V. Hoof, G. Borghs, G. Weimann, W. Schlapp, H. Nickel, and C. Klinshirn, Phys. Rev. B **43**, 4268 (1991).
[18] J.H. Shirley, Phys. Rev. **138**, 979 (1965).
[19] P.K. Tien and J.P. Gordon, Phys. Rev. **129**, 647 (1963).
[20] H. Drexler, J.S. Scott, S.J. Allen, K.L. Campman, and A.C. Gossard, Appl. Phys. Lett. **67**, 2816 (1995).